Monitoring of $CaCO_3$ Production on a Spinning Disc Reactor Using Conductivity Measurements

J. R. Burns
Protensive Ltd., International Centre for Life, Newcastle-upon-Tyne, Tyne & Wear, NE1 4EP, United Kingdom

R. J. J. Jachuck
Process Intensification & Clean Technology (PICT) Group, Dept. of Chemical Engineering, Clarkson University, Potsdam, NY 13699

DOI 10.1002/aic.10414
Published online March 31, 2005 in Wiley InterScience (www.interscience.wiley.com).

A method of monitoring $CaCO_3$ production from absorption of CO_2 into an aqueous solution of $Ca(OH)_2$ is described. Its application to the measurement of $Ca(OH)_2$ conversion across different radial zones on a spinning disc reactor is discussed and results from experiments are presented. Links between conversion and models based on diffusive mass transfer into a thin rotating film are examined and a correlation with Fourier and Reynolds numbers shown. Estimations of mass-transfer coefficients based on the experimental results are provided and comparisons made with previous work. © 2005 American Institute of Chemical Engineers *AIChE J,* 51: 1497–1507, 2005
Keywords: process intensification, spinning disc reactor, thin film, mass transfer, precipitation

Introduction

The growth in intensified processing has led to the creation of a range of reactors that offer environments with rapid heat and mass transfer capable of continuous processing, with residence times reduced to seconds rather than minutes or hours. Characterizing and modeling of the performance of these devices are often carried out through analysis of the output from the system, treating the reactor effectively as a "black box." Because of the short residence times involved in the actual process components, compared to the residence time within the system as a whole, this treatment can often lead to difficulties in isolating true performance characteristics from the possible unwanted end effects. Techniques that offer real-time local monitoring within the reaction environment can provide a much greater and more accurate insight into the performance of these reactors. The possibility of generating large data sets for the development of precise models is just one benefit of this approach.

Spinning disc reactors (SDRs) offer one avenue for process intensification through exploitation of high centrifugal acceleration to generate thin films providing rapid heat and mass transfer. Successful application of SDR technology to several chemical processes has been demonstrated, often leading to faster reaction and transport rates combined with improved yield and selectivity, as shown by Boodhoo and Jachuck[1] and Trippa et al.[2] In particular Trippa et al.[2] demonstrated the use of an SDR for the production of calcium carbonate particles from dissolved CO_2. The capability of this intensified system to generate a wide range of particle sizes and morphologies through control of the operating conditions, such as rotational speed, was clear. Analysis of the reaction, however, was limited to sampling the output from the system as a whole. Direct measurement of mass transfer or reaction rate within the rotating film was not obtained.

Previous studies of mass-transfer performance on an SDR were performed by Lim,[3] Moore,[4] and Auone and Ramshaw[5] providing data on gas–liquid mass-transfer coefficients, although results were often conflicting. Systems based on CO_2

Correspondence concerning this article should be addressed to R. J. J. Jachuck at rjachuck@clarkson.edu.

absorption, for example, gave results significantly different from those using O_2 absorption. Both Lim[3] and Auone and Ramshaw[5] used an invasive technique for sampling liquid from the disc while studying the absorption of O_2 into the liquid film. Their results implied a very strong link between rotation and mass transfer, with very high coefficients of up to 1 mm s^{-1} achievable. However, Moore[4] measured absorption of CO_2 in the exit stream and had to perform an extensive study to remove end effects from the calculations. The results indicated more moderate mass transfer with a much weaker link to rotational speed. There was therefore a clear scope for uncertainty in the existing mass-transfer models that could be used to study precipitation from a gas–liquid reaction, such as that for calcium carbonate production.

It was clear that a noninvasive method of directly monitoring calcium carbonate production on the disc surface would be of great benefit both to model the process on an SDR and to obtain more direct mass-transfer data. The work presented here describes one technique that can be used to provide these data.

Experimental Theory

In the following sections a method for monitoring the conversion of $Ca(OH)_2$ to $CaCO_3$ within a thin film using conductivity measurements will be described. The application of this technique to the case of thin film flow over a rotating disc will then be examined.

Mechanism of $CaCO_3$ formation from $Ca(OH)_2$ and CO_2

One common method of generating calcium carbonate is through the absorption and reaction of carbon dioxide (CO_2) with dissolved calcium hydroxide in an aqueous system. This reaction produces calcium carbonate ($CaCO_3$), which has a much lower solubility than that of either of the precursor components and thus precipitates out, usually in the form of small particles. The mechanisms involved in this process are fairly well understood and have been discussed in several reports such as those by Sherwood et al.,[6] Butler,[7] and Sullivan et al.[8] The following equations summarize the processes involved

$$CO_2 + H_2O \leftrightarrow H_2CO_3 \qquad (k_F \approx 1.1 \times 10^{-3}\ \text{L mol}^{-1}\ \text{s}^{-1}\ \text{at 25°C}) \quad (1)$$

$$CO_2 + OH^- \leftrightarrow HCO_3^- \qquad (k_F \approx 8 \times 10^{3}\ \text{L mol}^{-1}\ \text{s}^{-1}\ \text{at 25°C}) \quad (2)$$

$$HCO_3^- + OH^- \leftrightarrow CO_3^{2-} + H_2O \qquad (k_F \approx 6 \times 10^{9}\ \text{L mol}^{-1}\ \text{s}^{-1}) \quad (3)$$

$$Ca(OH)_2 \leftrightarrow Ca^{2+} + 2OH^- \quad (4)$$

$$CO_3^{2-} + Ca^{2+} \rightarrow CaCO_3 \quad (5)$$

Equation 1 describes the hydration of dissolved CO_2 to form weak carbonic acid. The forward reaction rate for this at 25°C is listed by Sullivan et al.[8] as 1.1×10^{-3} L mol^{-1} s^{-1}. In pure water this is described[7] as a slow reaction, giving an equivalent first-order rate of 0.06 s^{-1} for CO_2 conversion, yielding low concentrations of H_2CO_3, <0.1% of dissolved CO_2 at equilibrium. However, at higher pH values, where there are significantly more hydroxyl ions, such as in the presence of a strong base, the bicarbonate ion HCO_3^- can be formed rapidly by the direct reaction of CO_2 and OH^-, as shown by Eq. 2. Values for the forward reaction rate of this process were previously reported[6,7] and at 25°C the value is about 8×10^3 L mol^{-1} s^{-1}. The forward reaction rate for the formation of the carbonate ion, shown by Eq. 3, has been shown by Jolly[9] to be of the order of 6×10^9 L mol^{-1} s^{-1}, leading to rapid equilibrium times between the ions.

The dissociation of calcium hydroxide $Ca(OH)_2$ into Ca^{2+} ions and OH^- ions is shown in Eq. 4. In general this system is strongly dissociating and the majority of the calcium can be assumed to be in the form of Ca^{2+}. This results in liquid that is a strong base and will readily convert dissolved CO_2 into bicarbonate and carbonate ions that can rapidly react with the calcium ions, to form calcium carbonate $CaCO_3$, as illustrated in Eq. 5. The solubility of $CaCO_3$ in water at room temperature is very low at between 1.2×10^{-5} and 1.4×10^{-5} kg/kg as reported by Perry and Green[10] and readily precipitates out of the liquid as fine particles. This removes ions from the system and lowers both the pH and conductivity of the solution. The slow production of carbonic acid through the route shown by Eq. 1, after the complete conversion of the $Ca(OH)_2$, will continue to reduce the pH of the liquid and redissolve some of the $CaCO_3$, although this mechanism typically takes minutes and for short residence time processes, as described in this work, it can be ignored.

Reaction within the film on a rotating disc

If it is assumed that the reaction takes place within a thin film with CO_2 diffusing in from the upper surface and that the process is mass-transfer limited, then the liquid film can be divided into three distinct zones. The upper zone, depleted of Ca^{2+} and OH^- ions, should contain dissolved CO_2 along with $CaCO_3$. The lower zone of the film should contain mostly Ca^{2+} and OH^- ions from the remaining $Ca(OH)_2$. Separating these two zones will be a reaction zone in which CO_2 will react rapidly with hydroxyl and calcium ions to form $CaCO_3$, thus removing those ions from the liquid. An estimation of the characteristic thickness δ of the reaction zone for the simple case of a second-order reaction between two species A and B can be made by use of the following equation

$$\frac{D_A}{\delta} C_A = \frac{k_2 C_A C_{B0} \delta}{2} \quad (6)$$

In Eq. 6 it is assumed that the concentration of species B in the reaction zone is constant and has a value of C_{B0} and that species A is diffusing into the zone with a diffusion coefficient D_A and reacting with species B with a reaction rate constant of k_2. Using this approximate model, the thickness δ of the reaction zone can be estimated by

$$\delta = \sqrt{\frac{2D_A}{k_2 C_{B0}}} \quad (7)$$

Table 1. Experimental Conditions

Experiment	Liquid Flow (mL s^{-1})	Mean Liquid Flow (mL s^{-1})	Gas Flow (L min^{-1})	Rotational Speed (rpm)
1	5.6–6.6	6.0	10	200–1000
2	10.9–11.8	11.3	10	200–1000
3	20.9–21.6	21.4	15	200–1000

In the case of the reaction between CO_2 and $Ca(OH)_2$, depletions of both species will occur in the reaction zone; however, the order of magnitude of δ should remain close to that indicated by Eq. 7. To estimate k_2 the rate-limiting step of the sequence of reactions given in Eqs. 2–5 needs to be identified. Although data were not found for the reaction rate given by Eq. 5, it is considered to be near instantaneous. Assuming this to be true the rate of reaction of CO_2 in a $Ca(OH)_2$ aqueous solution should be limited by the process of bicarbonate ion formation, as shown in Eq. 2. In this case species A and B, represented in Eq. 7, can be assumed to be represented by CO_2 and OH^-, respectively.

Assuming a typical reaction temperature of 17°C, as was the case for the work presented here, the reaction rate constant for the bicarbonate ion formation should be about[6] 4.5 m^3 mol^{-1} s^{-1} and the diffusivity CO_2 in water[10] should be 1.7×10^{-9} m^2 s^{-1}. Assuming complete dissociation, the concentration of hydroxyl ions in the solution can be estimated to be twice that of the feed $Ca(OH)_2$ concentration. Taking a feed $Ca(OH)_2$ concentration typical of the experimental work of 18.7 mol m^{-3} would imply 37.4 mol m^{-3} of OH^-. Inserting these values into Eq. 7 would imply a characteristic thickness δ for the reaction zone under typical experimental conditions of 4.5 μm.

To examine how the thickness of the reaction zone compares to the film thickness in which the reaction takes place, a model for the film flow is required. The simplest and most common model used for predicting film thickness on a rotating disc is based on the Nusselt model.[11]

This gives film thickness h as a function of flow rate Q, rotational speed ω, radius r, and kinematic viscosity ν as reported by Burns et al.,[12] and can be written as

$$h = \left(\frac{3\nu Q}{2\pi r^2 \omega^2}\right)^{1/3} \tag{8}$$

Typical experimental conditions for the work presented here are shown in Tables 1 and 2. Using values typical of the experiments, Eq. 8 would imply a film thickness in the region of 28 to 430 μm. This is large compared to the characteristic reaction zone depth of 4.5 μm. The mass-transfer–limiting assumptions described in this section therefore should be expected to remain valid for the process of $CaCO_3$ formation within a film flowing over a rotating disc under the range of operating conditions examined here. This conclusion will be validated in the later discussion of the experimental results obtained from this study.

Table 2. Values of Parameters Used in Calculations

Parameter	Symbol	Values at 17°C
CO_2 diffusivity in water (D_A)	D_A	1.73×10^{-9} m^2 s^{-1}
Ca^2 diffusivity in water (D_B)	D_B	6.97×10^{-10} m^2 s^{-1}
CO_2 solubility in water (C_{A0})	C_{A0}	41 mol m^{-3}
Ca^2 feed concentration	C_{B0}	18.7 mol m^{-3}
Liquid feed kinematic viscosity	ν	1.5×10^{-6} m^2 s^{-1}
2nd-order reaction rate constant	k_2	9 m^3 mol^{-1} s^{-1}

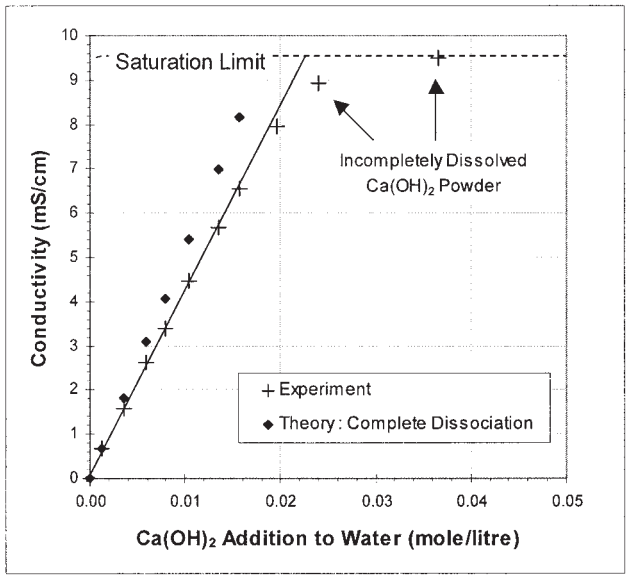

Figure 1. Measured relationship between conductivity and $Ca(OH)_2$ concentration.

Comparison made with theory based on complete dissociation of $Ca(OH)_2$.

Linking conductivity to $Ca(OH)_2$ concentration

The strong dissociation of calcium hydroxide in aqueous systems provides an ideal environment for linking electrical conductivity to concentration. In a system with only deionized water and calcium hydroxide the conductivity of the liquid can be related simply to the concentration of ions present as a result of the dissociation of $Ca(OH)_2$ into Ca^{2+} and OH^-. An experiment was performed to confirm this relationship for the $Ca(OH)_2$ supplied for this study. Powdered $Ca(OH)_2$ at 95% purity was added at various concentrations to deionized water at 18°C and mixed in a 4-L vessel. The conductivity was then measured using a handheld meter (Hanna Instruments, Woonsocket, RI). The results from this experiment are shown in Figure 1. A linear trend was observed, as expected, from the strongly dissociating $Ca(OH)_2$ and the best-fit empirical relationship is given as

$$S = \varepsilon[\mathrm{Ca(OH)_2}] \tag{9}$$

where $\varepsilon = 0.0414$ m^2 S^{-1} mol^{-1}.

This was compared with the theoretical conductivity that should be obtained from complete dissociation of $Ca(OH)_2$ into Ca^{2+} and $2OH^-$. Lide[13] lists the ionic conductivity of $0.5Ca^{2+}$ as 5.95×10^{-3} m^2 S^{-1} mol^{-1} and OH^- as 1.98×10^{-2} m^2 S^{-1} mol^{-1}, giving a theoretical conductivity of completely dissociated $Ca(OH)_2$ at low concentrations of 5.15×10^{-2} m^2 S^{-1} mol^{-1}. This value was 24% higher than that observed in Eq. 9 but did confirm the strong dissociation of $Ca(OH)_2$ into

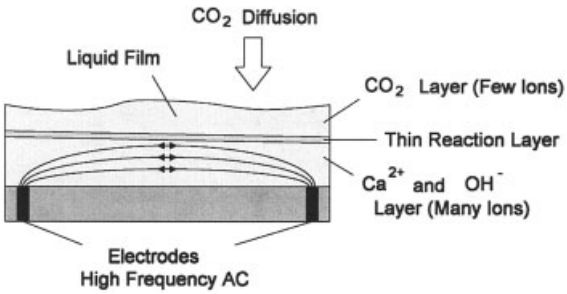

Figure 2. Measurement technique for monitoring ion concentration.

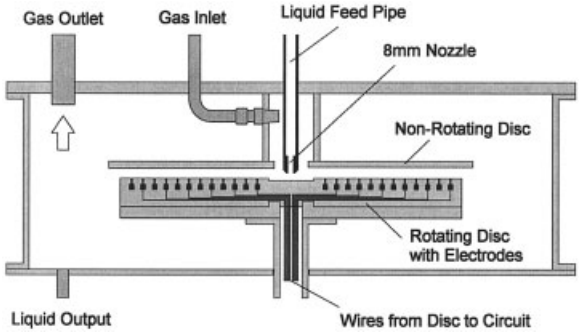

Figure 4. Spinning disc reactor configuration.

Ca^{2+} and OH^- and that its concentration could be linked easily to conductivity.

If it is assumed that the reaction layer within a film containing $Ca(OH)_2$ being converted to $CaCO_3$ is small compared to the film thickness, as implied in the previous section, then the remaining $Ca(OH)_2$ can be assumed to lie in a zone at the base of the film and be in the form of Ca^{2+} and OH^-. If the measurement of conductivity is taken from the base of the film, as illustrated in Figure 2, then the conductivity of the liquid should remain linked to the concentration of $Ca(OH)_2$ within the liquid film, as described by Eq. 9. Monitoring of conversion of CO_2 to $CaCO_3$ should therefore be possible through measurement of the conductivity using electrodes embedded in the surface at the base of the film.

Measurement of film conductivity on a rotating disc

The conductivity of the liquid film flowing over the disc was determined through measurements of the electrical resistance between electrodes embedded in the disc surface. The electrodes were mounted as concentric rings spaced at 1-cm-radial intervals, as shown in Figure 3. The spacing of the electrodes was much greater than the film thickness and so the electrical path through the liquid was approximately parallel to the disc surface. For a high-frequency alternating potential the electrical resistance between the electrodes can be written as[12]

$$R = \frac{1}{2\pi hS} \ln\left(\frac{r_2}{r_1}\right) \tag{10}$$

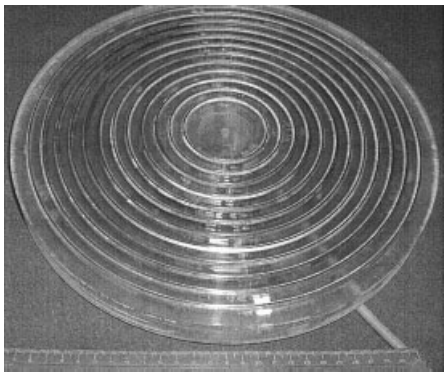

Figure 3. Perspex ™ disc with embedded concentric brass electrodes.

In Eq. 10, S is the conductivity and h is the thickness of the liquid film linking the two electrodes. An exact knowledge of film thickness h and geometry factors such as r_2 and r_1, however, is not essential in the measurement of conductivity if a calibration reading is taken for a liquid of the same film thickness but with a known conductivity. To achieve this, measurements of resistance were taken before monitoring $CaCO_3$ production using a nonreactive system in which the rotating disc flow was conducted under a blanket of nitrogen. Gas flow was then switched to pure carbon dioxide and a second set of readings taken, while maintaining the same flow and rotational speed. If it is assumed that the fluid environment, and thus film thickness, remains constant, then the ratio of resistance under nitrogen R_{N2} and under carbon dioxide R_{CO2} can be directly related to the ratio of conductivity S_{N2} and S_{CO2} by the following equation

$$\frac{S_{CO2}}{S_{N2}} = \frac{R_{N2}}{R_{CO2}} \tag{11}$$

If the conductivity of the liquid under nitrogen is assumed constant then the value of S_{N2} can be measured at the liquid source and used to calculate S_{CO2}. The assumption of unchanging geometrical conditions was expected to be a valid one because variations in flow rate, rotational speed, and liquid viscosity, arising from conversion to $CaCO_3$, were estimated to be relatively low. Indeed the viscosity of the solution at 100% conversion to $CaCO_3$ was measured to be at most 18% higher, and at a third-power influence on film thickness based on Eq. 8 it would contribute less than 5% error to the assumptions of Eq. 11.

Experimental Facility and Procedure

The equipment used to perform the experiments is illustrated in Figure 4. The system is essentially a modified version of the equipment previously discussed by Burns et al.[12] This consisted of a 30-cm rotating disc mounted within a 50-cm diameter stainless steel enclosure with a polypropylene (PP) lid. Liquid was pumped onto the disc through a pipe with an 8-mm nozzle using a centrifugal pump and controlled using a needle valve. The liquid flow rate was monitored using a turbine flow meter mounted in the feed line. Gas was fed cocurrently over the disc and was restricted by a PP static disc mounted about 10 mm above the rotating disc. This allowed equilibrium to be

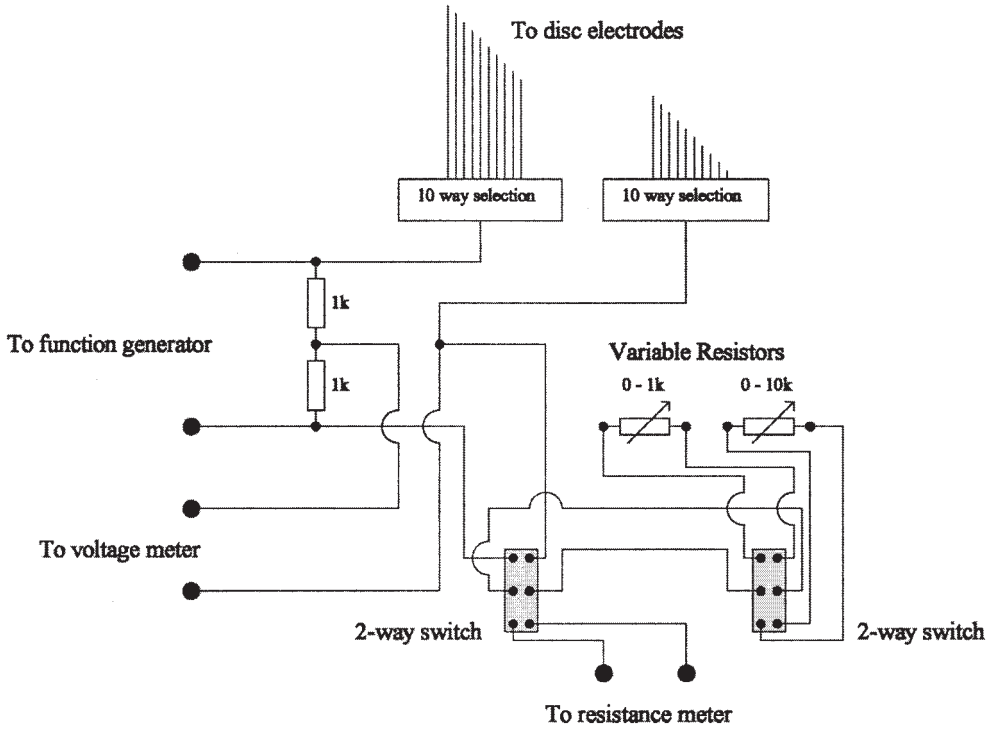

Figure 5. Circuit for measurement of conductance.

achieved quickly and, combined with the use of pure gases, helped ensure that gas-phase resistance was negligible.

Calcium hydroxide solutions were made in 4-L batches by mixing $Ca(OH)_2$ powder with deionized water to produce a solution of about 18.7 mol m^{-3} and 7.8 mS cm^{-1} conductivity. Several batches were produced and poured into a feed tank, to make a total volume of nearly 16 L. This was done just before the experiments to minimize pre-disc conversion to $CaCO_3$ resulting from the slow reaction with CO_2 in the atmosphere. Conductivity was monitored in the feed tank throughout the experimentation and no noticeable changes were found, indicating pre-disc reaction to be insignificant.

The Perspex ™ disc used for the experiments, described in the previous section and shown in Figure 3, had 12 electrodes mounted at 1-cm-radial intervals from 3- to 14-cm radius. The first 11 electrodes were used in this study and were connected to an electrical circuit, shown in Figure 5, by a slip-ring assembly. Measurements of resistance were made through a technique of bridge balancing against two multiturn potentiometers whose ranges are 1–10 kΩ. A high-frequency function generator (TG120 20-MHz function generator) was used to supply a 2-V potential at 2 kHz using a sine wave form. This was used to ensure the liquid behaved as a resistor obeying Ohm's law. A voltmeter (IVM100 1-MHz AC volt meter, Iso-Tech, Derby, UK) was connected to the circuit to monitor the voltage across the bridge. Because both the function generator and the voltmeter were grounded it was necessary to pass the load from the function generator through a unity gain transformer to isolate its output from the ground and allow correct metering of the voltage.

Experimental conditions used are summarized in Table 1. Nitrogen was initially used for each experiment and ten resistance readings were taken between the inner 11 rings. This was achieved by switching the circuit through each pair of rings in turn and balancing the bridge at each point. The resistance used to balance the bridge was measured by switching it into a circuit with a resistance meter. The gas was then changed to pure CO_2 and 1 min allowed for equilibrium to be established before a second set of readings was taken. The ratio of resistance combined with the input conductivity was used to calculate the conductivity between each pair of rings, as shown in Eq. 11. The conversion of $Ca(OH)_2$ was then calculated from the change in conductivity and a graph produced showing this change across the surface of the rotating disc.

A total of 21 experiments were performed to examine $CaCO_3$ production on an SDR. Seven rotational speeds were used: 200, 300, 400, 500, 600, 800, and 1000 rpm. Three liquid flow rates were used: about 6, 11, and 21 mL s^{-1} with a carbon dioxide flow of 10 to 15 L min^{-1}. This delivered about 7 to 11 mmol s^{-1} of CO_2 compared with a maximum of 0.4 mmol s^{-1} of $Ca(OH)_2$ in the liquid. Combined with the relatively low gas velocity of <0.3 m s^{-1} this ensured that CO_2 pressure, and therefore concentration, could be assumed to remain constant at the film interface and therefore mass transfer to be limited purely to the liquid film side.

Results and Analysis

Performance of the SDR for the conversion of $Ca(OH)_2$ to $CaCO_3$ is illustrated in Figure 6 for a subset of experimental conditions. It can be seen that complete conversion was achievable on this unit when low flows and high rotational speeds were used. Based on the Nusselt flow model it can be shown that timescales in the region of 0.2 to 0.5 s were required to achieve complete conversion. The detection limit shown in Figure 7 indicates the point at which electrical resistance ex-

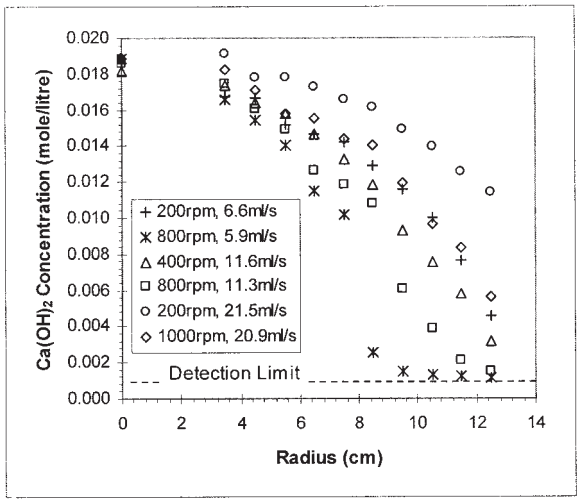

Figure 6. Measurements of calcium hydroxide concentration from a selection of experimental conditions.

Values based on conductance measured between different radial zones.

ceeded the range of the balancing circuit, typically after around 95% conversion, and so points along this line should be taken to be upper limits of concentration.

Analysis of the performance of the system was made using several common measures based on diffusive transport models. These are discussed in the following sections.

Modeling diffusive transport within the rotating flow

The equations for mass transfer by diffusion have been studied and solved for many simple systems. One of the most comprehensive studies of this process was given by Crank[14] in which the equations for diffusion are examined for several generalized systems. In the simple case of diffusion in one dimension the equation can be written as

$$u\frac{\partial C}{\partial x} = D\frac{\partial^2 C}{\partial z^2} \tag{12}$$

For this simple case convective flux arising from velocity u in the x-axis is balanced against diffusion perpendicular to the flow in the z-axis. This is commonly reduced to the following dimensionless form using a length scale L for the x-axis, Z for the z-axis, and u_M for the flow velocity

$$u'\frac{\partial C'}{\partial x'} = \mathrm{Fo}\frac{\partial^2 C'}{\partial z'^2} \qquad \text{where Fo} = \left(\frac{DL}{u_M Z^2}\right) \tag{13}$$

This process can therefore be described purely in terms of the dimensionless Fourier number (Fo) along with appropriate boundary conditions. When combined with a reaction, as is the case for $CaCO_3$ formation, the process becomes more complex. For the case of a second-order reaction between species A and B, Eq. 12 can be modified to

$$u\frac{\partial C_i}{\partial r} = D_i\frac{\partial^2 C_i}{\partial z^2} - k_2 C_A C_B \qquad \text{for } i = \text{A, B} \tag{14}$$

To apply this equation to the case of a thin film over a rotating disc a model is required for the liquid flow. Assuming a fully developed laminar film of thickness h and mean velocity u_M, the radial velocity profile for the liquid can be assumed to be of the following form[15]

$$u = \frac{3}{2}u_M\left(\frac{2z}{h} - \frac{z^2}{h^2}\right) \tag{15}$$

The mean velocity of the film can be linked to the liquid flow rate using the following expression

$$u_M = \frac{Q}{2\pi r h} \tag{16}$$

In the case of flow over the rotating disc the film thickness h is itself a function of disc radius. Assuming that film thickness across the disc follows the Nusselt model, as defined by Eq. 8, the following scaling relationships can be used to relate Eq. 14 to the case of thin film flow over a rotating disc

$$C_i = C_i' C_{i0} \qquad \text{for } i = \text{A, B} \tag{17}$$

$$r = r' r_2 \tag{18}$$

$$z = z' h = \frac{z'}{r'^{2/3}}\left(\frac{3\nu Q}{2\pi^2 r_2^2 \omega^2}\right)^{1/3} \tag{19}$$

$$u = \frac{3}{2}u_M(2z' - z'^2) = \left(\frac{9Q^2\omega^2}{32\pi^2 r_2 \nu}\right)^{1/3}\frac{(2z' - z'^2)}{r'^{1/3}} \tag{20}$$

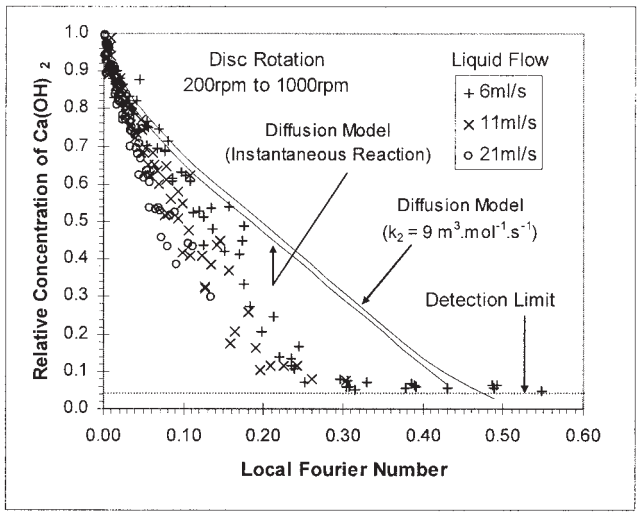

Figure 7. Measured calcium hydroxide concentration compared with feed concentration.

Data correlated with local Fourier number.

Applying this scaling to Eq. 14 produces the following dimensionless form

$$(2z' - z'^2)\frac{\partial C_i'}{\partial r'} = \mathrm{Fo}_i r'^{5/3}\frac{\partial^2 C_i'}{\partial z'^2} - K_i C_\mathrm{A}' C_\mathrm{B}' r'^{1/3} \qquad i = \mathrm{A, B} \tag{21}$$

The dimensionless groups governing this equation are

$$\mathrm{Fo}_i = \left(\frac{128\pi^4}{81}\right)^{1/3}\left(\frac{\omega^2 r_2^8 D_i^3}{\nu Q^4}\right)^{1/3} \qquad i = \mathrm{A, B} \tag{22}$$

$$K_\mathrm{A} = \left(\frac{32\pi^2}{9}\right)^{1/3}\left(\frac{r_2^4 k_2^3 C_{\mathrm{B}0}^3 \nu}{Q^2\omega^2}\right)^{1/3} \tag{23}$$

$$K_\mathrm{B} = \left(\frac{32\pi^2}{9}\right)^{1/3}\left(\frac{r_2^4 k_2^3 C_{\mathrm{A}0}^3 \nu}{Q^2\omega^2}\right)^{1/3} \tag{24}$$

Equation 22 provides an equivalent definition for the Fourier number for the case of film flow over the rotating disc surface and should therefore govern the effectiveness of diffusive transport axially through the film. The other groups K_A and K_B represent the comparative performance of the reaction to deplete concentration. For the limiting case of $K_i \rightarrow \infty$ the overlap in the species of A and B within the film will tend to zero and the observed reaction rate should be limited by the diffusive transport into the reaction zone that is governed by the Fourier numbers on each side of the zone.

Comparison of results with the diffusive transport model

A comparison of the experimental results with the diffusive transport model, described by Eq. 21, was made. As previously discussed it was assumed that the two molecules limiting transport into the reaction zone were the diffusion of CO_2 in the upper part of the film and the diffusion of Ca^{2+} in the lower part of the film, as illustrated in Figure 2. The following definitions for species A and B in the diffusive transport model were therefore made

$$C_\mathrm{A} = [\mathrm{CO_2}] \tag{25}$$

$$C_\mathrm{B} = [\mathrm{Ca^{2+}}] \tag{26}$$

The boundary conditions for the $CaCO_3$ process applied to Eq. 21 were

$$C_\mathrm{A}' = 1 \qquad \text{at } z' = 1 \tag{27}$$

$$C_\mathrm{A}' = 0 \qquad C_\mathrm{B}' = 1 \qquad \text{at } r' = r_1/r_2 \tag{28}$$

$$\frac{\partial C_\mathrm{B}'}{\partial z'} = 0 \qquad \text{at } z' = 0, z' = 1 \tag{29}$$

$$\frac{\partial C_\mathrm{A}'}{\partial z'} = 0 \qquad \text{at } z' = 0 \tag{30}$$

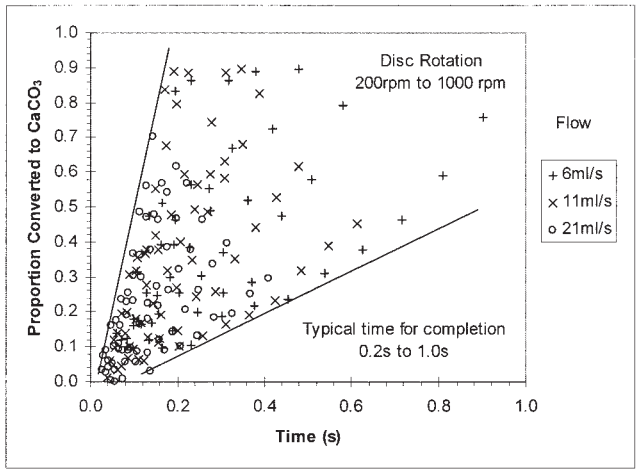

Figure 8. Comparison of conversion of calcium hydroxide to calcium carbonate with residence time based on Nusselt flow model.

Values for the constants used in Eqs. 21–24 were taken from experimental conditions at a typical feed temperature of 17°C based on data from the literature.[6,10,13] The value for the k_2 constant was derived from the assumed limiting step described in Eq. 2. The value of the forward reaction rate constant given by Sherwood et al.,[6] based on a temperature of 17°C, was 4.5 $m^3\ mol^{-1}\ s^{-1}$. Assuming that $[OH^-] \approx 2[Ca^{2+}]$ in the local reaction zone, this gave an effective second-order rate constant k_2 for this model of 9 $m^3\ mol^{-1}\ s^{-1}$.

Numerical solutions of Eq. 21 for species A and B were computed for the range of experimental conditions shown in Table 1. The method used divided the film into 20 axial cells and stepped through the solution from $r' = (r_1/r_2)$ to $r' = 1$ using 10,000 radial steps. For the limiting case of $K_i \gg \mathrm{Fo}_i$, results from the numerical solutions can be strongly correlated against the local Fourier number defined as

$$\mathrm{Fo} = \mathrm{Fo}_\mathrm{A} r'^{5/3} = \left(\frac{128\pi^4}{81}\right)^{1/3}\left(\frac{\omega^2 r^8 D_\mathrm{A}^3}{\nu Q^4}\right)^{1/3} \tag{31}$$

Experimental results for $Ca(OH)_2$ conversion were observed to correlate strongly against the local Fourier number as defined by Eq. 31. Figure 7 shows $Ca(OH)_2$ conversion as a function of local Fourier number. Two comparison lines based on the numerical solution of Eq. 21 were included: the first for the limiting case of $k_2 \rightarrow \infty$ and the second showing the averaged solution, across the experimental range, for the case of $k_2 = 9$ $m^3\ mol^{-1}\ s^{-1}$.

The results showed a good correlation between Fourier number and conversion and that for a Fourier number > 0.15 the conversion to $CaCO_3$ generally exceeded 92%. This result was highly useful in confirming that the process was strongly linked to diffusive mass transfer, as assumed in the previous discussion. The results, however, did indicate reaction rates of between 1.6 and 2.8 times faster than those predicted, even for the limiting case of $k_2 \rightarrow \infty$. Overall, this suggested that the transport mechanism was driven strongly by molecular diffusion but with some enhancement arising from axial convection,

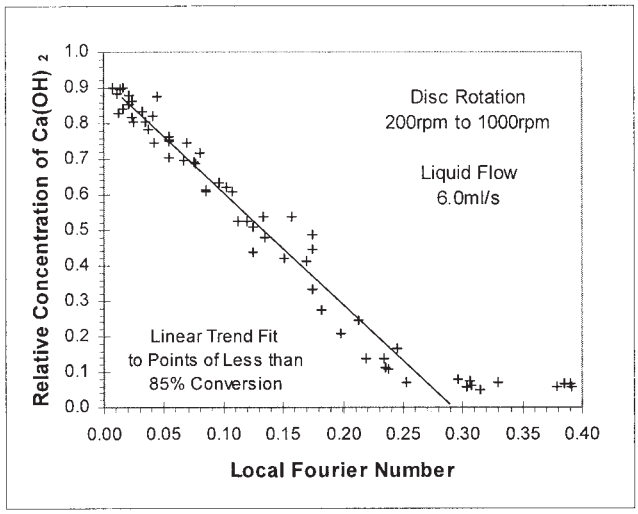

Figure 9. Correlation between conversion and local Fourier number for the lowest liquid flow rate.

probably caused by the action of surface waves as described by Sisoev et al.[16]

The enhancement ascribed to additional axial convective transport processes appeared to be most noticeably influenced by the liquid flow rate over the disc and less influenced by the rotational speed. The results from the experiments were therefore isolated into groups covering the three flow rates examined. Conversions of $Ca(OH)_2$ for the three cases were plotted against local Fourier number and the results are shown in Figures 8, 9, and 10, respectively. The most notable influence of flow was the change in the gradient of the line linking conversion to Fourier number. A linear fit was applied to the data to quantify this effect. Intercepts of the zero concentration line were measured and the results are listed in Table 3. This indicated that at the highest flow rate of 21 mL s^{-1} complete conversion would be obtained typically for a local Fourier

Table 3. Calculated Fourier Intercepts for Complete Conversion of $Ca(OH)_2$

Data Set	Local Fourier Intercept
Experiment 1	0.29
Experiment 2	0.22
Experiment 3	0.17
Diffusion model (infinite reaction)	0.46

number of 0.17, compared to 0.29 for the case of the lowest flow rate of 6 mL s^{-1}. This was compared with the diffusion model that indicated complete conversion should be obtained for a Fourier number of 0.46 in the limiting case of $k_2 \rightarrow \infty$.

Conversion of $Ca(OH)_2$ to $CaCO_3$ was also compared with residence time, based on the Nusselt flow model, and the results are shown in Figure 11. This was used first to quantify the observed reaction performance achievable by this process and second to examine any limiting influence of residence time on conversion. The results showed no clear correlation between conversion and residence time. This further pointed to the process being mass-transfer limited and that the transport rates within the thin film had not yet reached the limitations of the reaction kinetics.

Best-fit empirical correlation for $CaCO_3$ production

The final analysis performed on the data was to examine the best-fit empirical model of conversion in terms of the three operating variables: radius, rotational speed, and liquid flow rate. The data set examined was restricted to conversions of $<85\%$, where a good fit could be obtained from simple regression analysis. This reduced the data set from 210 points to 190. The resulting best fit correlation found was

$$[CaCO_3] \propto r^{2.23}\omega^{0.49}Q^{0.89} \tag{32}$$

Confidence intervals for the exponents are given in Table 4. This correlation was compared with the strong link with local

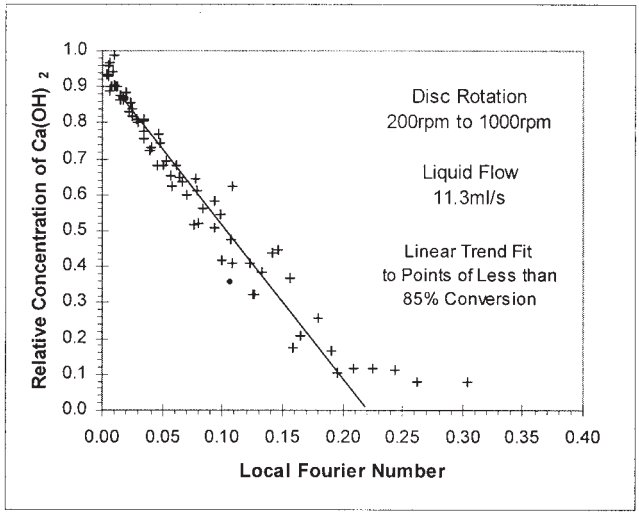

Figure 10. Correlation between conversion and local Fourier number at the medium liquid flow rate.

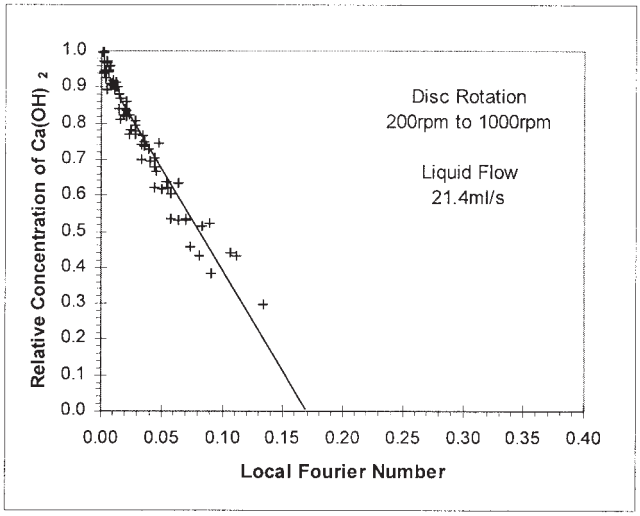

Figure 11. Correlation between conversion and local Fourier number at the highest liquid flow rate.

Table 4. Exponents of Operating Parameters in Empirical Model for $CaCO_3$ Production

Parameter	Best Fit	Lower 95% Limit	Upper 95% Limit
Radius	0.49	0.38	0.59
Rotational speed	2.23	2.09	2.37
Liquid flow rate	−0.89	−1.00	−0.78

Fourier number shown in the previous analysis. Combining Eqs. 31 and 32 gave

$$[\mathrm{CaCO_3}] \propto \mathrm{Fo}\left(\frac{Q}{r\omega^{0.4}}\right)^{0.44} \tag{33}$$

A residual nondiffusive transport influence was observed in this correlation that appears to be a strong function of liquid flow and radius and a weaker function of rotational speed. This residual influence was expected to be the result of an axial convective transport process and thus a link to Reynolds number was sought. For flow over a rotating disc, the Reynolds number can be written as

$$\mathrm{Re} = \frac{u_M h}{\nu} = \frac{Q}{2\pi r} \tag{34}$$

Combining Eqs. 33 and 34 gives

$$[\mathrm{CaCO_3}] \propto \mathrm{Fo}\,\mathrm{Re}^{0.44}\omega^{-0.17} \tag{35}$$

This empirical relationship indicated that a combination of the influence of Fourier and Reynolds groups could be used to characterize the observed production rate of $CaCO_3$ within the thin film flow over the rotating disc. However, the residual rotational speed influence on the conversion to $CaCO_3$ remains, although this may be explained by additional factors characteristic of the nature of the convective mechanisms, such as surface wave frequency and amplitude. The rotational speed influence may also be indicative of a small kinetic limitation because increased rotational speed will reduce the residence time of the film on the disc.

Mass-Transfer Performance

Estimating the mass-transfer coefficient

The flux of CO_2 through the gas–liquid interface can be written in terms of the reaction enhanced mass-transfer coefficient k^*_{LG} using the following equation

$$\mathrm{Flux} = k^*_{LG} A \Delta C_{LMCD} \tag{36}$$

where A is the surface area of the film and ΔC_{LM} is the log mean concentration difference, defined as

$$\Delta C_{LM} = \frac{(\Delta C_{A1} - \Delta C_{A2})}{\ln(\Delta C_{A1}/\Delta C_{A2})} \tag{37}$$

The total transfer of CO_2 through the interface can be most easily defined at the point at which complete conversion is achieved. Flux at that point can be written as

$$\mathrm{Flux} = Q(C_{B0} + \alpha C_{A0}) \tag{38}$$

where α is the proportion of CO_2 dissolved in the film compared with its solubility C_{A0}. ΔC_{LM} can be computed in terms of α using the following equations

$$\Delta C_{A1} = C_{A0} \qquad \text{and} \qquad \Delta C_{A2} = (1 - \alpha) C_{A0} \tag{39}$$

Therefore

$$\Delta C_{LM} = \left[\frac{\alpha C_{A0}}{-\ln(1 - \alpha)}\right] \tag{40}$$

The area A required to complete the reaction can be defined in terms of the local Fourier number at the point of completion using the following relationship

$$A = \pi r^2 = \left(\frac{81\mathrm{Fo}^3 \nu Q^4}{128\omega^2 D_A^3}\right)^{1/4} \tag{41}$$

By combining these equations, k^*_{LG} can be computed from

$$k^*_{LG} = \left(\frac{128\omega^2 D_A^3}{81\mathrm{Fo}^3 \nu}\right)^{1/4} \left(\frac{C_{B0}}{\alpha C_{A0}} + 1\right) \ln\left(\frac{1}{1 - \alpha}\right) \tag{42}$$

The equivalent mass-transfer coefficient without reaction k_{LG} can be calculated from k^*_{LG} in terms of the enhancement factor E using

$$k_{LG} = \frac{k^*_{LG}}{E} \tag{43}$$

For infinite reaction with no gas-phase resistance the enhancement factor E can be written as given by Levenspiel[17]

$$E = 1 + \frac{D_B C_{B0}}{D_A C_{A0}} \tag{44}$$

Inserting data from Table 2 for the experiments reported here gives an enhancement factor $E = 1.184$. Assuming a diffusive mass-transfer process the concentration of CO_2 in the film at the point of completion can be estimated from numerical solutions of Eq. 21. These indicate that α should be approximately 0.33 at completion. By inserting the projected values of the local Fourier number for complete conversion, as listed in Table 3, along with $\alpha = 0.33$ and $E = 1.184$ into Eqs. 42 and 43, values for mass-transfer coefficients can be computed for each of the liquid flow rates examined. Results of this analysis are shown in Figure 12.

Comparison with previous studies

Lim[3] and Auone and Ramshaw[5] both examined mass transfer from measurements of O_2 uptake into a deoxygenated liquid. Lim[3] made measurements at various radial locations from 6 to 18 cm with liquid flows of 15 to 61 mL s^{-1}. Reported results for a flow of 21 mL s^{-1} gave mass-transfer coefficients

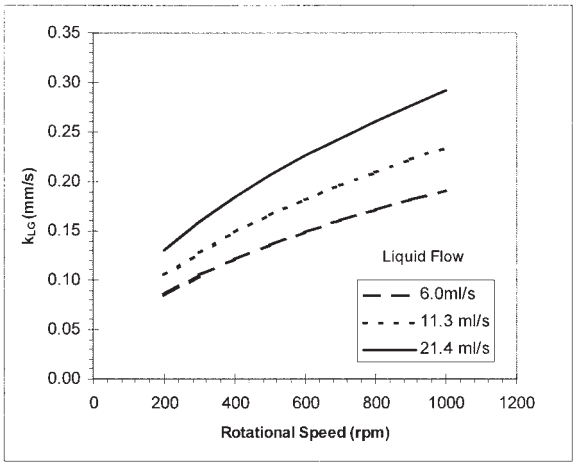

Figure 12. Calculated gas–liquid mass-transfer coefficients based on Fourier number at the completion of the reaction.

in the range of 0.16 mm s^{-1} at 227 rpm up to 0.97 mm s^{-1} at 1100 rpm. At low speeds some rough agreement in values can be seen, although the steep increase at higher speeds is almost triple that observed in Figure 12. A similar conclusion was drawn, in agreement with the work of Aoune and Ramshaw.[5]

Moore[4] conducted studies at substantially higher flows of between 50 and 100 mL s^{-1}; however, the results conflict strongly with those of Lim.[3] Mass-transfer coefficients were in the range of 0.20 mm s^{-1} at 50 mL s^{-1} flow at 500 rpm up to 0.42 mm s^{-1} for 100 mL s^{-1} flow at 1500 rpm. Assuming a continued trend in increasing k_{LG} with flow, as shown in a comparison of curves in Figure 12, then a value of 0.28 mm s^{-1} would be expected for a flow of 50 mL s^{-1} at 500 rpm. In general, neither of the previous studies afforded a good match to the observations of this study with the results shown in Figure 12, lying between the two extremes of Lim[3] and Moore.[4]

Conclusions

The results from this work have shown that electrical conductivity can be used to monitor the consumption of calcium hydroxide during the formation of calcium carbonate. The data generated have indicated that complete conversion can be obtained for solutions containing 19 mol m^{-3} of $Ca(OH)_2$ within a single pass over a 30-cm disc. No indication of a significant kinetic limitation has been reached herein, with residence times as low as 0.2 s being able to achieve complete conversion and gas–liquid mass-transfer coefficients reaching 0.3 mm s^{-1}. However data on the reaction rate constants provided in the background literature suggest that this may eventually occur at higher rotational speeds if a film thickness of a few microns were reached.

The more general advantage of rotational speed in increasing conversion has been clearly shown with increased conversion obtained at higher speeds. This was expected from the improved effectiveness of diffusion in the thinner films. This has highlighted the benefit of centrifugal acceleration as a tool for increasing throughput within smaller volumes, one key element in the philosophy of process intensification.

The use of in situ measurements providing data in real time may also offer opportunities for both the development of more accurate models and the creation of control systems capable of operating within the short residence time constraints of intensified processing equipment. In the case of SDRs this could lead to improved tailoring of the reaction environment for systems in which ion composition is linked to conversion.

In the specific case of commercial bulk $CaCO_3$ production higher strength feed stocks containing undissolved quantities of $Ca(OH)_2$ are more commonly used alongside mixed gas feeds containing lower concentrations of CO_2. These introduce additional complexities and limitations—such as dissolution rates, formation of $CaCO_3$ at the surface of calcium hydroxide particles, and gas-side mass-transfer resistance—that may reduce the ability of an SDR process to achieve complete conversion over a single pass. However, the ability of the SDR to provide a more controlled environment for particle production may provide benefits in the higher value end of the market.

Acknowledgment

The authors would like to thank EPSRC, U.K. for providing funding for this work under the IMI Program.

Notation

A = surface area of film, m^2
C = concentration of species, mol m^{-3}
ΔC = concentration difference, mol m^{-3}
ΔC_{LM} = log mean concentration difference, mol m^{-3}
D = diffusion coefficient, m^2 s^{-1}
E = enhancement factor in mass transfer attributed to reaction
Fo = dimensionless Fourier number
h = film thickness, m
h_R = effective film thickness for electrical conductance, m
k_L = internal liquid mass-transfer coefficient, m s^{-1}
k_{LG} = gas–liquid mass-transfer coefficient, m s^{-1}
k^*_{LG} = gas–liquid mass-transfer coefficient with reaction enhancement, m s^{-1}
K = dimensionless group governing reaction rate
L = length scale for diffusion, m
Q = volumetric flow rate of liquid, m^3 s^{-1}
r = radial coordinate
R = electrical resistance, Ω
Re = dimensionless Reynolds number
S = electrical conductivity, S m^{-1}
t = time, s
t_c = characteristic time for diffusion, s
t_{res} = residence time, s
u = radial velocity, m s^{-1}
u_M = mean radial velocity, m s^{-1}
x = distance in the direction of flow, m
Z = axial length scale for diffusion, m

Greek letters

δ = characteristic thickness of reaction zone, m
ε = ionic conductivity of liquid, m^2 S^{-1} mol^{-1}
ν = kinematic viscosity of liquid, m^2 s^{-1}
ω = speed of disc rotation, rad s^{-1}

Subscripts

1 = condition at start of process
2 = condition at end of process
A = relating to species A (CO_2)
B = relating to species B [Ca^{2+} or $Ca(OH)_2$]
CO2 = relating to conditions under CO_2
N2 = relating to conditions under nitrogen

Superscript

′ = equivalent dimensionless value

Acronym

SDR = spinning disc reactor

Literature Cited

1. Boodhoo KVK, Jachuck RJ. Process intensification: Spinning disc reactor for condensation polymerization. *Green Chem.* 2000;2:235-244.
2. Trippa G, Hetherington P, Jachuck RJJ. Process intensification: Precipitation of calcium carbonate from the carbonation reaction of lime water using a spinning disc reactor, Proc of 15th Int Symp on Industrial Crystallisation, Sorrento, Italy; 2002.
3. Lim ST. *Hydrodynamics and Mass Transfer Processes Associated with the Absorption of Oxygen in Liquid Films Flowing across a Rotating Disc*. PhD Thesis, University of Newcastle-upon-Tyne, UK; 1980:162-173.
4. Moore SR. *Mass Transfer into Thin Liquid Films with and without Chemical Reaction*. PhD Thesis, University of Newcastle-upon-Tyne, UK; 1986:137-185.
5. Auone A, Ramshaw C. Process intensification: Heat and mass transfer characteristics of liquid films on rotating discs. *Int J Heat Mass Transfer*. 1999;42:2543-2556.
6. Sherwood TK, Pigford RL, Wilke CR. *Mass Transfer*. New York, NY: McGraw-Hill; 1975:361-371.
7. Butler JN. *Carbon Dioxide Equilibria and Their Applications*. Chelsea, MI: Lewis Publishers; 1991:Chapters 2 and 4.
8. Sullivan BP, Krist K, Guard HE. *Electrochemical and Electrocatalytic Reactions of Carbon Dioxide*. Amsterdam: Elsevier; 1993:6-7.
9. Jolly WL. *Modern Inorganic Chemistry*. New York, NY: McGraw Hill; 1985:194-195.
10. Perry RH, Green D. *Perry's Chemical Engineers' Handbook*. 6th ed. Chemical Engineering Series. New York, NY: McGraw-Hill International Editions; 1984.
11. Nusselt W. Die Oberflächenkondensation des Wasserdampfes. *Z Ver deut Ing*. 1916;60:541.
12. Burns JR, Ramshaw C, Jachuck RJJ. Measurement of liquid film thickness and the determination of spin-up radius on a rotating disc using an electrical resistance technique. *Chem Eng Sci.* 2003;58:2245-2253.
13. Lide DR. *CRC Handbook of Chemistry and Physics*. 75th ed. Boca Raton, FL: CRC Press; 1995.
14. Crank J. *The Mathematics of Diffusion*. 2nd ed. Oxford, UK: Clarendon Press; 1975:44-68.
15. Holland FA. *Fluid Flow for Chemical Engineers*. London: Edward Arnold; 1973:220-221.
16. Sisoev GM, Matar OK, Lawrence CJ. Axisymmetric wave regimes in viscous liquid film flow over a spinning disk. *J Fluid Mech*. 2003;495:385-411.
17. Levenspiel O. *Chemical Reaction Engineering*. 2nd ed. New York, NY: Wiley; 1976:411-417.

Manuscript received Mar. 21, 2004, and revision received Aug. 25, 2004.